AGU ADVANCING EARTH AND SPACE SCIENCES

Geophysical Research Letters

RESEARCH LETTER
10.1029/2024GL109241

The Impact of Vertical Plasma Motion on the Evolution of Predawn Equatorial Plasma Bubbles on the Dayside

Hyosub Kil[1], **Joseph D. Huba**[2], **and Larry J. Paxton**[1]

[1]The Johns Hopkins University Applied Physics Laboratory, Laurel, MD, USA, [2]Syntek Technologies, Fairfax, VA, USA

Key Points:

- Evolution of predawn equatorial plasma bubbles on the dayside is investigated using Sami3 is Another Model of the Ionosphere
- Bubbles generated at predawn persist into the dayside, and their transport to higher altitudes by vertical motion prolongs their lifetime
- Bubbles maintain their field-aligned characteristics during their evolution on the dayside in the presence of vertical plasma motion

Correspondence to:
H. Kil,
hyosub.kil@jhuapl.edu

Citation:
Kil, H., Huba, J. D., & Paxton, L. J. (2024). The impact of vertical plasma motion on the evolution of predawn equatorial plasma bubbles on the dayside. *Geophysical Research Letters*, *51*, e2024GL109241. https://doi.org/10.1029/2024GL109241

Received 12 MAR 2024
Accepted 20 APR 2024

Author Contributions:
Conceptualization: Joseph D. Huba
Formal analysis: Joseph D. Huba
Methodology: Joseph D. Huba
Software: Joseph D. Huba
Validation: Larry J. Paxton
Writing – review & editing: Joseph D. Huba, Larry J. Paxton

Abstract This study investigates the impact of vertical ionospheric drift during daytime on the evolution of predawn equatorial plasma bubbles by conducting model simulations using "Sami3 is Another Model of the Ionosphere." The upward drift of the ionosphere transports bubbles to higher altitudes, where their lifetime is set by the atomic oxygen photoionization rate. While the bubbles generated at predawn persist into dayside, the bubbles generated shortly after sunset diminish before sunrise. Therefore, post-sunset bubbles do not contribute to daytime electron density irregularities. Bubbles maintain their field-aligned characteristics throughout the daytime regardless of the vertical ionospheric drift. This property allows bubbles to exist near the magnetic equator despite poleward plasma transport by the fountain process. The shift of irregularity concentration to higher latitudes over time in satellite observations is explained by the combined effect of transport of bubbles to higher altitudes and rapid refilling of depletions near the magnetic equator.

Plain Language Summary The Earth's equatorial ionosphere becomes turbulent at night, manifested in the phenomenon known as equatorial spread F (ESF). During ESF large-scale electron density depletions (often referred to as "bubbles") develop and low-density plasma is transported to higher altitudes. While bubbles are primarily nighttime phenomena, some persist longer and evolve into sources of electron density irregularities on the dayside. Bubbles are concentrated near the magnetic equator at night in satellite observations, but during the daytime, their peak occurrence frequency shifts to higher latitudes over time. This phenomenon is attributed to the latitudinal redistribution of bubbles in association with the vertical motion of the ionosphere. We assess this hypothesis by conducting numerical simulations. The simulation results reveal that the field-aligned characteristics of bubbles are maintained during the plasma redistribution process. This property provides a valuable tool for understanding the daytime behavior of bubbles as observed by satellites.

1. Introduction

The equatorial F region ionosphere experiences turbulence at night due to the action of the generalized Rayleigh-Taylor instability (Huba, 2022; Huba et al., 2008; Sultan, 1996; Yokoyama, 2017). Following sunset, the rapid decrease in E region plasma density renders the bottomside of the F region ionosphere susceptible to the Rayleigh-Taylor instability. This instability leads to the upward transport of low-density plasma from lower altitudes to higher altitudes, where the plasma density is higher. The term "bubbles" denotes plasma depletions or irregularities in plasma density generated by this process (Woodman & La Hoz, 1976). These bubbles typically form shortly after sunset, correlating with intensified upward motion of the ionosphere near the sunset terminator (Anderson et al., 2004; Fejer et al., 1999; Kil et al., 2009; Smith et al., 2015). However, the timeframe for bubble development varies depending on season, solar cycle, and geomagnetic activity. Bubbles develop late at night under certain conditions such as geomagnetic storms and low solar activity (Aa et al., 2020; Ajith et al., 2021; Heelis et al., 2010; Smith & Heelis, 2017; Stoneback et al., 2011; Watthanasangmechai et al., 2016; Yizengaw et al., 2013). Rapid refilling of bubbles occurs after sunrise through photoionization, causing bubbles to be predominantly detected during nighttime.

While most bubbles disappear after sunrise, some persist into the daytime and become sources of daytime electron density irregularities in the topside ionosphere (He et al., 2023; Huang et al., 2013; Kil et al., 2019; Otsuka et al., 2021; Xie et al., 2020). A notable characteristic of irregularities detected during the daytime by satellites is shift of their concentration from the magnetic equator to higher latitudes over time (Kil et al., 2019, 2020). This observation is attributed to the latitudinal redistribution of bubbles caused by the fountain effect, which involves upward plasma motion and subsequent diffusion to higher latitudes (Balan et al., 2017; Hanson & Moffett, 1966). The correlation between the latitudinal distribution of daytime irregularities and vertical plasma velocity is

suggested as supporting evidence for this interpretation (Kil et al., 2020). However, this observation does not corroborate the role of the fountain effect because the transport of irregularities from the equatorial region to higher latitudes along magnetic field lines has not yet been verified through observation. Additionally, the absence of irregularities near the magnetic equator at satellite altitudes does not necessarily imply the absence of irregularities at other altitudes. Numerical simulations are required to assess the evolution of bubbles on the dayside in the presence of vertical plasma motion.

This study investigates the impact of the fountain effect on bubble evolution during the daytime by conducting numerical simulation with SAMI3/ESF (Sami3 is Another Model of the Ionosphere/equatorial spread F) model (Huba et al., 2008). We examine the evolution of a bubble initiated at 04:00 local time (LT) in both the absence and presence of vertical plasma motion on the dayside. The role of the fountain effect is assessed by comparing the outcomes from these simulations. The properties of bubbles that we are interested in identifying from numerical simulations include their field-aligned characteristics and lifetime during the course of their evolution on the dayside. Additionally, we explore the evolution of a bubble initiated at 19:00 LT to assess the contribution of post-sunset bubbles to daytime irregularities.

2. Model Description

The three-dimensional ESF code SAMI3/ESF (Huba et al., 2008) is used in this study. This model is based on the global SAMI3 model (Huba & Joyce, 2010) but limited to a narrow longitude range. The following geophysical parameters are used for this study: F10.7 = 135, F10.7A = 135, and Ap = 4 for 21 September 2017. The plasma is modeled from hemisphere to hemisphere up to 24° in magnetic latitude. The magnetic apex heights range from 90 to 1,250 km, and the longitudinal width is 4° (i.e., 460 km). The grid is (nz, nf, nl) = (204, 192, 288) where nz is the number of grid points along each magnetic field line, nf is the number of grid points in latitude, and nl is the number grid points in longitude. This altitude grid is variable and has a resolution of 1–20 km from 90 to 1,250 km. The longitude grid has a resolution of 0.014° (i.e., 1.6 km). In essence we are simulating a narrow "wedge" of the ionosphere at night. A Gaussian-like ion density perturbation was imposed at time zero. For all simulations, we used a peak ion density of the perturbation of 50% centered at 2° longitude with a half-width of 0.25°, at an altitude of 286 km with a half-width of 30 km. We set neutral winds to zero.

3. Results

Model simulations were conducted around 8°E magnetic longitude on 21 September 2017. Simulation results for other seasons were not presented in this study, as the simulations in September suffice to demonstrate the influence of vertical ionospheric motion on bubble evolution. For our experiment, we initiated bubbles at 04:00 LT by artificially setting vertical plasma velocity to zero. These bubbles had fully matured before sunrise, enabling us to track their evolution on the dayside. However, the initiation time and generation conditions of bubbles are not critical factors for our study. Different spatial scales and depletion depths of bubbles develop at various times under different conditions. Larger bubbles initiated earlier can persist longer on the dayside than smaller bubbles initiated later. While we cannot simulate the evolution of all types of bubbles numerically, our experiment with bubbles initiated at 04:00 LT suffices for the purpose of this study. This is because the effect of daytime vertical drift on the field-aligned characteristics and lifetime of bubbles identified in our experiment is commonly applicable to any bubbles persisting into the dayside, irrespective of their initiation time and generation conditions at night.

Figure 1 illustrates three different conditions of vertical plasma motion perpendicular to the electric (**E**) and magnetic (**B**) fields (i.e., $\mathbf{E} \times \mathbf{B}$ drift), which were employed to represent the background ionosphere motion. In Run 1, $\mathbf{E} \times \mathbf{B}$ drift was set to zero (black solid) throughout the day. For Run 2, the Scherliess and Fejer (SF) model (Scherliess & Fejer, 1999) was employed by substituting zero for the downward velocity (red dashed line). Run 3 utilized the full SF model $\mathbf{E} \times \mathbf{B}$ drift (green solid). The vertical dotted lines indicate the initiation times of bubbles for Runs 1 and 2 (04:00 LT) and Run 3 (19:00 LT).

Runs 1 and 2 (04:00 LT bubble initiation) are designed to investigate the impact of $\mathbf{E} \times \mathbf{B}$ drift on dayside bubble evolution. According to the SF model, the $\mathbf{E} \times \mathbf{B}$ drift is typically downward at night. Since the bubble initiated at 04:00 LT does not grow under this condition, we set the $\mathbf{E} \times \mathbf{B}$ drift to zero instead of utilizing the SF model conditions. We artificially modified the $\mathbf{E} \times \mathbf{B}$ drift to generate bubbles at predawn, but zero vertical velocity at predawn and development of bubbles under this condition are not unrealistic situations (Heelis et al., 2010;

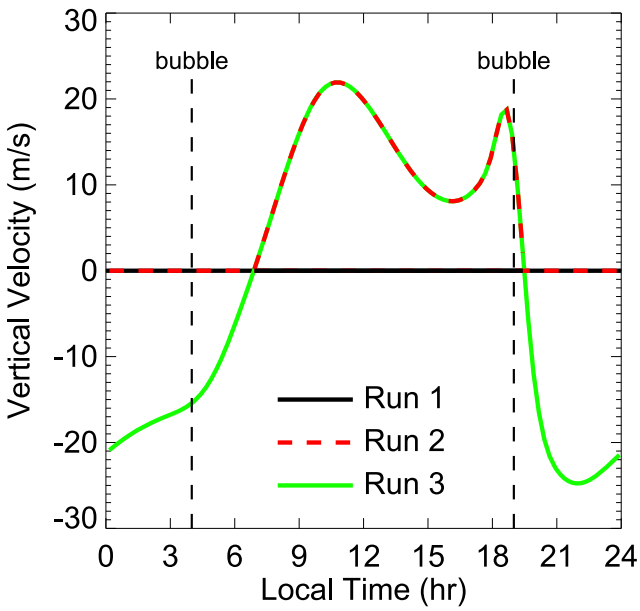

Figure 1. Vertical $\mathbf{E} \times \mathbf{B}$ drift models employed for three runs. $\mathbf{E} \times \mathbf{B}$ drift is zero throughout for Run 1 (black solid). Run 2 (red dashed) employes SF model by setting the downward velocity to zero after about 18 LT. Run 3 (green solid) utilizes the full SF model $\mathbf{E} \times \mathbf{B}$ drift. The initiation times of perturbations are indicated by vertical lines. Model simulations were conducted around 8°E magnetic longitude on 21 September 2017.

Stoneback et al., 2011). A high occurrence rate of irregularities in the post-midnight sector is observed in regions where the $\mathbf{E} \times \mathbf{B}$ drift is upward or weakly downward at night. Bubbles can grow under these conditions because cooling of the atmosphere late at night positively influences bubble growth by reducing the ion-neutral collision rate (Heelis et al., 2010). Runs 1 and 2 represent bubble evolution in the absence and presence of the fountain effect, respectively. Run 3 aims to investigate the persistence of a bubble at night, observing the evolution of one initiated at 19:00 LT.

In Figure 2, we examine the influence of the fountain effect on bubble evolution by comparing the outputs obtained from (a–d) Run 1 and (e–h) Run 2 at four different LTs (hh:mm): 06:00, 09:00, 12:00, and 15:00. Each figure represents a cross-section of the density in the vertical and zonal planes at the magnetic equator. Figures 2a and 2e at 06:00 LT are identical because the vertical $\mathbf{E} \times \mathbf{B}$ drift has not yet begun to differ. By 06:00 LT, the fully developed bubble reaches an altitude of approximately 750 km. This altitude remains consistent throughout the day in Figures 1b–1d due to the absence of vertical $\mathbf{E} \times \mathbf{B}$ drift in Run 1. Conversely, in Figures 2f–2h, the upper boundary of the bubble progressively increases, surpassing 1,200 km by 15:00 LT.

From these results, several noteworthy aspects are observed. First, the disappearance of bubble signatures occurs earlier at lower altitudes. This phenomenon is attributed to the rapid refilling of bubbles at lower altitudes through photoionization. Second, the longevity of bubble signatures in Figures 2f–2h, compared to Figures 2b–2d, suggests an extension in the lifetime of bubbles due to the influence of the vertical $\mathbf{E} \times \mathbf{B}$ drift of the ionosphere. The sustained presence of bubbles at higher altitudes is linked to the slower refilling caused by a low photoionization rate (Otsuka et al., 2021). Third, bubble signatures at lower altitudes vanish more quickly in Figures 2f–2h than in Figures 2b–2d due to the upward motion of the background ionosphere in Figures 2f–2h. Because the bubble moves upward with the background in Figures 2f–2h, bubble signatures naturally disappear from lower altitudes. Another reason for the early disappearance of bubbles at lower altitudes in Figures 2f–2h is the difference in the background density between Figures 2b–2d and 2f–2h. The upward motion of the ionosphere creates a plasma density reduction in the equatorial region by the fountain effect. Comparing the densities at the same altitudes in Figures 2d and 2h reveals that below ~500 km altitude, Figure 2d exhibits a higher plasma density, while above ~500 km, Figure 2h exhibits a greater plasma density. In regions with higher background plasma density, plasma refilling within depletions takes longer. The presence of bubble signatures below 500 km altitude even at 15:00 LT in Figure 2d is attributed to the high background plasma density.

The simulation results in Figure 2 indicate that the bubble generated at 04:00 LT persists throughout the day irrespective of the presence of the fountain effect, although the fountain effect does extend the bubble's lifetime at higher altitudes. While bubbles developed late at night serve as sources of daytime electron density irregularities, those formed shortly after sunset (referred to as post-sunset bubbles) can also contribute to daytime irregularities. To investigate this further, we examine the evolution of a post-sunset bubble initiated at 19:00 LT over the course of the night.

Figure 3, a cross-section of the density in the vertical and zonal planes at the magnetic equator, shows the results of the post-sunset bubble simulation (Run 3) at four different LTs: (a) 21:00, (b) 02:00, (c) 05:00, and (d) 06:00. Three figures are shown after midnight, as the primary focus of the simulation lies in observing the persistence of the bubble until sunrise. By around 21:00 LT, the bubble growth ceases, with Figure 3a depicting the fully developed bubble reaching an altitude of approximately 900 km. As time elapses, the ionosphere, encompassing the bubble, contracts to a narrow altitude range, concurrent with the decay of the bubble itself. The contraction of the ionosphere occurs due to its downward motion and the subsequent reduction in density throughout the night. Bubble signatures are still visible at 05:00 LT, yet they dissipate by 06:00 LT following sunrise.

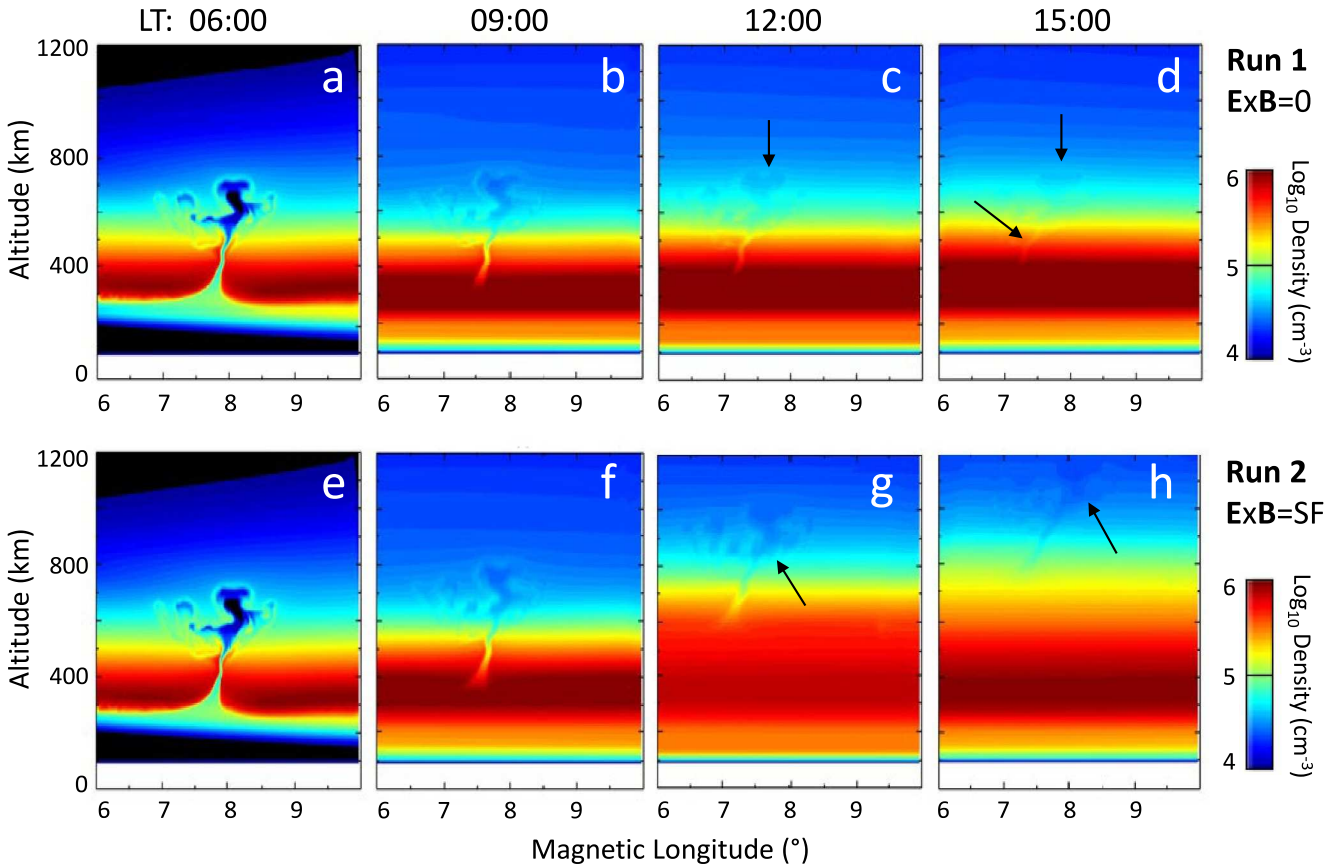

Figure 2. Comparison of the outcomes of (a–d) Run 1 and (e–h) Run 2 at four different LTs (hh:mm): 06:00, 09:00, 12:00, and 15:00. Each figure represents a cross-section of the density in the vertical and zonal planes at the magnetic equator. Arrows are used to aid in the recognition of weak bubble signatures at 12:00 and 15:00 LTs.

4. Discussion

The model simulation results provide insights into interpreting bubble detections in satellite observations. Typically, the occurrence rate of bubbles reaches its peak before midnight (Aa et al., 2020; Kil & Heelis, 1998; Stolle et al., 2006), naturally decreasing thereafter due to their decay. However, as depicted in Figure 3, the decline in the occurrence rate over time in the topside can also result from the ionosphere's contraction. In the

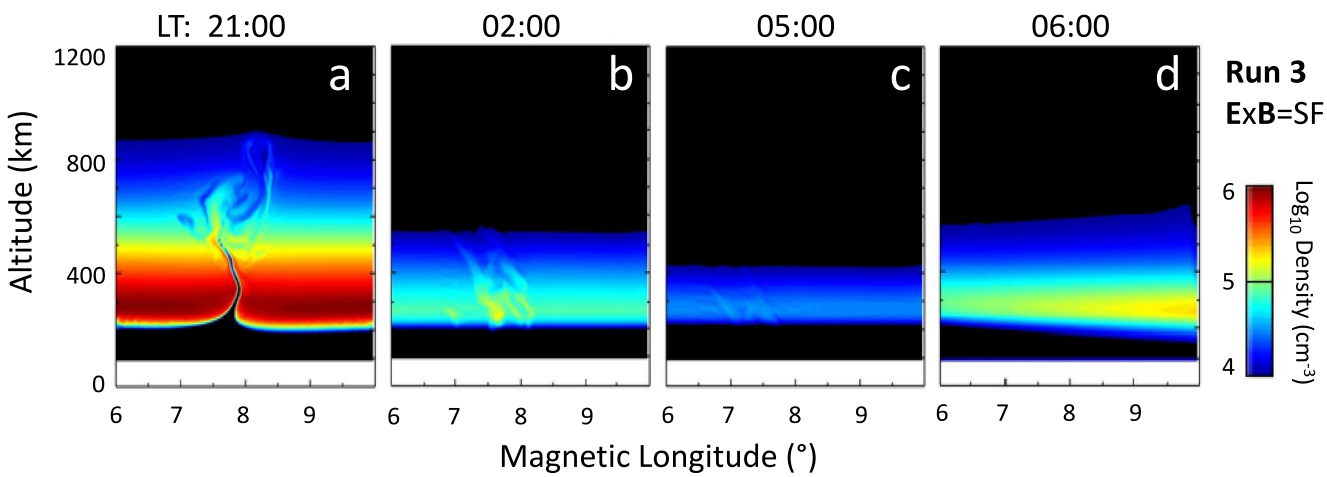

Figure 3. Run 3 outcomes at four different LTs (hh:mm): (a) 21:00, (b) 02:00, (c) 05:00, and (d) 06:00. Each figure represents a cross-section of the density in the vertical and zonal planes at the magnetic equator.

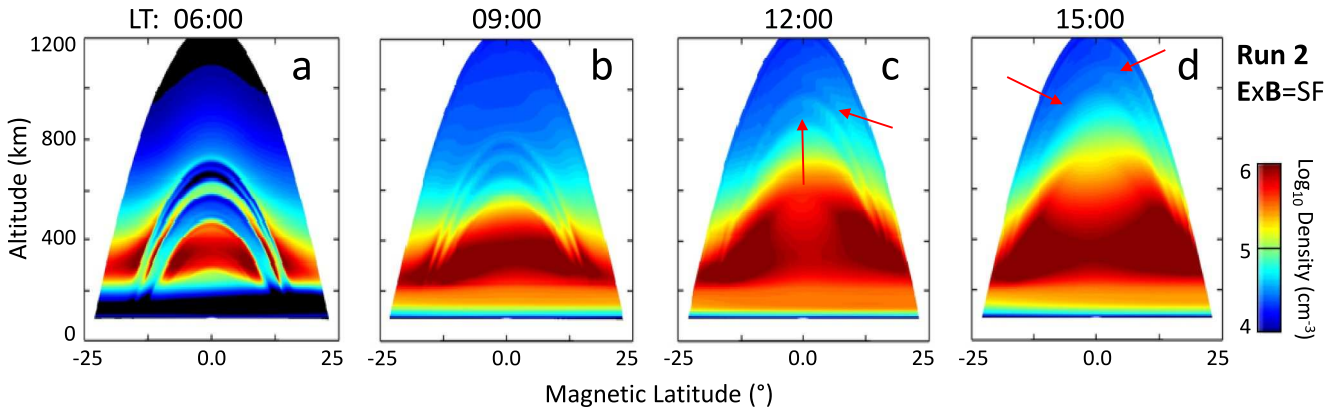

Figure 4. Run 2 outcomes at four different LTs (hh:mm): (a) 06:00, (b) 09:00, (c) 12:00, and (d) 15:00. Each figure represents a cross-section of the density in the vertical and latitude planes at 8°E. Arrows are used to aid in the recognition of field-aligned depletions at 12:00 and 15:00 LTs.

scenario presented in Figure 3, if a satellite samples the ionosphere at 600 km altitude, it would be unable to detect irregularities at 02:00 LT and later, primarily because of the ionosphere's contraction. In contrast, a satellite positioned at 300 km altitude would detect bubble signatures even at 05:00 LT. It is essential to keep in mind that the decrease in the occurrence rate of bubbles over time in satellite observations is not solely attributed to their decay.

In previous studies (Kil et al., 2019, 2020), the shift of irregularity concentration from the magnetic equator to higher latitudes over time was attributed to their redistribution by the fountain effect. When we consider the ambient plasma, this redistribution indicates the transport of plasma from the equatorial region to higher latitudes following magnetic field lines. This process leads to the formation of an ionization trough around the magnetic equator and ionization crests outside the magnetic equator. Similarly, the poleward shift of irregularity concentration in satellite observations can be interpreted as a consequence of the poleward transport of irregularities around the magnetic equator. However, the redistribution of bubbles differs from that of ambient plasma because bubbles constitute elongated structures along magnetic field lines.

We assess the maintenance of field-aligned properties of bubbles on the dayside by examining cross-sections of the density in the vertical and latitudinal planes. Figure 4 presents cross-sections at the magnetic longitude 8°E, generated using the Run 2 conditions at four different LTs: (a) 06:00, (b) 09:00, (c) 12:00, and (d) 15:00. Due to the tilt and division of the bubble into several branches, not all field lines are filled with depletions at the specified longitude. Bubble signatures, as illustrated in the figures, are identified as field-aligned structures. Therefore, the fountain effect does not affect the distinctive bubble characteristics.

Because bubbles maintain field-aligned characteristics, bubble signatures do not disappear from the equatorial region due to the fountain effect; rather, they survive longer in the equatorial region due to their transport to higher altitudes. The latitudinal extent of bubbles is greater at lower altitudes due to the geometry of the magnetic field lines and field-aligned nature of bubbles. As bubbles move upward with the background ionosphere, a satellite encounters a lower (wider) part of bubbles. This effect explains the poleward shift of irregularity concentration over time. Bubble signatures at the same altitude persist longer into the dayside outside the equatorial region because the refilling by photoionization occurs slower at higher latitudes. The reduction of the background ionospheric density in the equatorial region by the fountain process further facilitates the fast refilling of depletions around the magnetic equator. Because the vertical **E×B** drift of the ionosphere is more significant near the magnetic equator than outside, bubbles could be lifted beyond satellite altitudes around the magnetic equator. The lack of irregularities in the equatorial region in satellite observations is attributed to these factors.

5. Conclusions

The evolution of equatorial plasma bubbles during the daytime in the presence of vertical ionospheric motion is investigated using the SAMI3/ESF model. Bubbles generated at predawn persist into the dayside, becoming sources of daytime electron density irregularities. However, bubbles generated shortly after sunset diminish before sunrise. The vertical motion of the ionosphere during the daytime transports bubbles to higher altitudes,

where their lifetime is prolonged. The high concentration of daytime irregularities beyond the magnetic equator in satellite observations was attributed to the transport of bubbles from the equatorial region to higher latitudes by the fountain process. However, bubbles do not disappear in the equatorial region by the fountain process because they maintain field-aligned characteristics throughout their evolution; instead, they last longer in the equatorial region in the presence of vertical ionospheric motion. The scarcity of bubble signatures near the magnetic equator during the daytime in satellite observations is primarily due to the transport of bubbles beyond satellite altitudes and fast refilling of depletions around the magnetic equator due to low background plasma density. Our simulation results provide insight into the interpretation of satellite observations at night as well as on the dayside. Bubbles move downward at night in accordance with the downward motion of the ionosphere. A part of the decrease in the bubble occurrence rate with time at night in satellite observations is related to the transport of bubbles below satellite altitudes.

Data Availability Statement

The SAMI3 model is available from SAMI3-Software (2024). Three simulation results distinguished by filenames are available from SAMI3-Results (2024).

Acknowledgments
This work is supported by NSF-AGS2029840 and NASA-NNH19ZDA001N. J. Huba also acknowledges the support by NASA 80NSSC21K1305.

References

Aa, E., Zou, S., & Liu, S. (2020). Statistical analysis of equatorial plasma irregularities retrieved from Swarm 2013–2019 observations. *Journal of Geophysical Research: Space Physics*, *125*(4), e2019JA027022. https://doi.org/10.1029/2019JA027022

Ajith, K. K., Ram, S. T., Li, G. Z., Yamamoto, M., Hozumi, K., Yatimi, C. Y., & Supnithi, P. (2021). On the solar activity dependence of midnight equatorial plasma bubbles during June solstice periods. *Earth and Planetary Physics*, *5*(5), 378–386. https://doi.org/10.26464/epp2021039

Anderson, D. N., Reinisch, B., Valladares, C., Chau, J., & Veliz, O. (2004). Forecasting the occurrence of ionospheric scintillation activity in the equatorial ionosphere on a day-to-day basis. *Journal of Atmospheric and Solar-Terrestrial Physics*, *66*(17), 1567–1572. https://doi.org/10.1016/j.jastp.2004.07.010

Balan, N., Souza, J., & Bailey, G. J. (2017). Recent developments in the understanding of equatorial ionization anomaly: A review. *Journal of Atmospheric and Solar-Terrestrial Physics*, *171*, 3–11. https://doi.org/10.1016/j.jastp.2017.06.020

Fejer, B. G., Scherliess, L., & de Paula, E. R. (1999). Effects of the vertical plasma drift velocity on the generation and evolution of equatorial spread F. *Journal of Geophysical Research*, *104*(A9), 19859–19869. https://doi.org/10.1029/1999JA900271

Hanson, W. B., & Moffett, R. J. (1966). Lonization transport effects in the equatorial F region. *Journal of Geophysical Research*, *71*(23), 5559–5572. https://doi.org/10.1029/JZ071i023p05559

He, Z., Chen, G., Yan, C., Zhang, S., Yang, G., Li, Y., et al. (2023). Imaging radar observations of the daytime F-region irregularities in low-latitudes of China. *Journal of Geophysical Research: Space Physics*, *128*(2), e2022JA030878. https://doi.org/10.1029/2022JA030878

Heelis, R. A., Stoneback, R., Earle, G. D., Haaser, R. A., & Abdu, M. A. (2010). Medium-scale equatorial plasma irregularities observed by coupled ion-neutral dynamics investigation sensors aboard the communication navigation outage forecast system in a prolonged solar minimum. *Journal of Geophysical Research*, *115*(A10), A10321. https://doi.org/10.1029/2010JA015596

Huang, C.-S., de La Beaujardiere, O., Roddy, P. A., Hunton, D. E., Ballenthin, J. O., & Hairston, M. R. (2013). Long-lasting daytime equatorial plasma bubbles observed by the C/NOFS satellite. *Journal of Geophysical Research: Space Physics*, *118*(5), 2398–2408. https://doi.org/10.1002/jgra.50252

Huba, J. D. (2022). Generalized Rayleigh-Taylor instability: Ion inertia, acceleration forces, and E region drivers. *Geophysical Research Letters*, *127*(6), e2022JA030474. https://doi.org/10.1029/2022JA030474

Huba, J. D., & Joyce, G. (2010). Global modeling of equatorial plasma bubbles. *Geophysical Research Letters*, *37*(17), L17104. https://doi.org/10.1029/2010GL044281

Huba, J. D., Joyce, G., & Krall, J. (2008). Three-dimensional equatorial spread F modeling. *Geophysical Research Letters*, *35*(10), L10102. https://doi.org/10.1029/2008GL033509

Kil, H., & Heelis, R. A. (1998). Global distribution of density irregularities in the equatorial ionosphere. *Journal of Geophysical Research*, *103*(A1), 407–417. https://doi.org/10.1029/97JA02698

Kil, H., Lee, W. K., & Paxton, L. J. (2020). Origin and distribution of daytime electron density irregularities in the low-latitude F region. *Journal of Geophysical Research: Space Physics*, *125*(9), e2020JA028343. https://doi.org/10.1029/2020JA028343

Kil, H., Paxton, L. J., Lee, W. K., & Jee, G. (2019). Daytime evolution of equatorial plasma bubbles observed by the first Republic of China satellite. *Geophysical Research Letters*, *46*(10), 5021–5027. https://doi.org/10.1029/2019GL082903

Kil, H., Paxton, L. J., & Oh, S.-J. (2009). Global bubble distribution seen from ROCSAT-1 and its association with the pre-reversal enhancement. *Journal of Geophysical Research*, *114*(A6). https://doi.org/10.1029/2008JA013672

Otsuka, Y., Shinbori, A., Sori, T., Tsugawa, T., Nishioka, M., & Huba, J. D. (2021). Plasma depletions lasting into daytime during the recovery phase of a geomagnetic storm in May 2017: Analysis and simulation of GPS total electron content observations. *Earth and Planetary Physics*, *5*, 427–434. https://doi.org/10.26464/epp2021046

SAMI3-Results. (2024). Sami3 model simulation results [Dataset]. https://doi.org/10.5281/zenodo.10500752

SAMI3-Software. (2024). Sami3 model source codes [Software]. https://doi.org/10.5281/zenodo.7895859

Scherliess, L., & Fejer, B. G. (1999). Radar and satellite global equatorial *F* region vertical drift model. *Journal of Geophysical Research*, *104*(A4), 6829–6842. https://doi.org/10.1029/1999JA900025

Smith, J., & Heelis, R. A. (2017). Equatorial plasma bubbles: Variations of occurrence and spatial scale in local time, longitude, season, and solar activity. *Journal of Geophysical Research: Space Physics*, *122*(5), 5743–5755. https://doi.org/10.1002/2017JA024128

Smith, J. M., Rodrigues, S. F., & de Paula, E. R. (2015). Radar and satellite investigations of equatorial evening vertical drifts and spread F. *Annales Geophysicae*, *33*(11), 1403–1412. https://doi.org/10.5194/angeo-33-1403-2015

Stolle, C., Lühr, H., Rother, M., & Balasis, G. (2006). Magnetic signatures of equatorial spread F as observed by the CHAMP satellite. *Journal of Geophysical Research*, *111*(A2), A02304. https://doi.org/10.1029/2005JA011184

Stoneback, R. A., Heelis, R. A., Burrell, A. G., Coley, W. R., Fejer, B. G., & Pacheco, E. (2011). Observations of quiet time vertical ion drift in the equatorial ionosphere during the solar minimum period of 2009. *Journal of Geophysical Research*, *116*(A12), A12327. https://doi.org/10.1029/2011JA016712

Sultan, P. J. (1996). Linear theory and modeling of the Rayleigh-Taylor instability leading to the occurrence of equatorial spread F. *Journal of Geophysical Research*, *101*(A12), 26875–26891. https://doi.org/10.1029/96JA00682

Watthanasangmechai, K., Yamamoto, M., Saito, A., Tsunoda, R., Yokoyama, T., Supnithi, P., et al. (2016). Predawn plasma bubble cluster observed in Southeast Asia. *Journal of Geophysical Research: Space Physics*, *121*(6), 5868–5879. https://doi.org/10.1002/2015JA022069

Woodman, R. F., & La Hoz, C. (1976). Radar observations of F region equatorial irregularities. *Journal of Geophysical Research*, *81*(31), 5447–5466. https://doi.org/10.1029/JA081i031p05447

Xie, H., Yang, S., Zhao, X., Hu, L., Sun, W., Wu, Z., et al. (2020). Unexpected high occurrence of daytime F-region backscatter plume structures over low latitude Sanya and their possible origin. *Geophysical Research Letters*, *47*(22). https://doi.org/10.1029/2020gl090517

Yizengaw, E., Retterer, J., Pacheco, E. E., Roddy, P., Groves, K., Caton, R., & Baki, P. (2013). Postmidnight bubbles and scintillations in the quiet-time June solstice. *Geophysical Research Letters*, *40*(21), 5592–5597. https://doi.org/10.1002/2013GL058307

Yokoyama, T. (2017). A review on the numerical simulation of equatorial plasma bubbles toward scintillation evaluation and forecasting. *Progress in Earth and Planetary Science*, *4*(1), 37. https://doi.org/10.1186/s40645-017-0153-6